Quantum anomalous Hall effect in metal-bis(dithiolene), magnetic properties, doping and interfacing graphene

F. Crasto de Lima, Gerson J. Ferreira, and R. H. Miwa
Instituto de Física, Universidade Federal de Uberlândia,
C.P. 593, 38400-902, Uberlândia, MG, Brazil
(Dated: May 31, 2018)

The realization of the Quantum anomalous Hall effect (QAHE) in two dimensional (2D) metal organic frameworks (MOFs), $(MC_4S_4)_3$ with M = Mn, Fe, Co, Ru and Rh, has been investigated based on a combination of first-principles calculations and tight binding models. Our results for the magnetic anisotropy energy (MAE) reveal that the out-of-plane (in-plane) magnetization is favored for M = Mn, Fe, and Ru (Co, and Rh). Given the structural symmetry of $(MC_4S_4)_3$, the QAHE takes place only for M = Mn, Fe and Ru. Such a quantum anomalous Hall phase has been confirmed through the calculation of the Chern number, and examining the formation of topologically protected (metallic) edge states. Further electron (n-type) doping of the MOFs has been done in order to place the Fermi level within the non-trivial energy gap; where we find that in $(RuC_4S_4)_3$, in addition to the up-shift of the Fermi level, the MAE energy increases by 40%. Finally, we show that in MOF/graphene (vdW) interfaces, the Fermi level tunning can be done with an external electric field, which controls the charge transfer at the MOF/graphene interface, giving rise to switchable topologically protected edge currents in MOFs.

I. INTRODUCTION

Since the theoretical proposal of the quantum spin Hall (QSH) phase in graphene[1], the search, as well as the control, of the topological phases in two dimensional (2D) systems has been the subject of intense studies over the past few years. For instance, investigations addressing 2D materials characterized by larger and tuneable (non-trivial) energy gaps mediated by mechanical strain[2], external electric field perpendicular to the 2D sheet ($EEF_\perp$)[3], and/or suitable chemical combinations[4]. Further studies have been done focusing on the van der Waals (vdW) heterostructures by stacking 2D topological insulators (TI), and combinations of trivial/topological materials[5].

In a seminal work, Wang *et al.*[6] predicted the quantum anomalous Hall effect (QAHE) in a metal organic framework (MOF) composed by benzene rings attached to three-fold coordinated Mn atoms. Different topological phases have been identified in other MOFs, like the QSH phase in nickel-bis-dithiolene $[(NiC_4S_4)_3]$[7], synthesized by Kambe *et al.*[8]; and the QAHE in manganese-bis-dithiolene $[(MnC_4S_4)_3]$[9]. In the latter, the topological phase has been changed from QSH to QAH by replacing the metallic element, Ni→Mn. On the other hand, keeping the transition metal and changing the organic host, recent theoretical studies predicted that $(MnC_3S_6)_3$ can be tuned from a Chern insulator to Chern half-metal as a function of the Fermi level[10]. In parallel, currently we are facing an amazing progress on the synthesis of 2D metal frameworks[11]. For instance, the synthesis of metal (M) bis-dicyanobenzenedithiolate with M = Fe, Co, Ni, Pd, Pt, and Zn[12], which is somewhat similar to the metal bis-dithiolene. Further molecular design has been done by building up multilayered systems by stacking MOFs[13–16]. Very recently, based on first-principles calculations, we have found that bilayer systems of $(MC_4S_4)_3$, with M=Ni and Pt, present the Z_2-metallic phase, where the edge states can be tuned by an $EEF_\perp$[17].

In contrast with its counterpart, the time-reversal symmetric QSH phase, the breaking of this symmetry by intrinsic magnetization rules the emergence of the QAHE. Such an additional ingredient can be used to control the the electronic properties and the topological phases in 2D systems. Indeed, by tuning the strength of the exchange field, we may have different types of topological gaps and half-metallic phases induced by (intra/inter) spin orbit couplings (SOCs)[18,19]. Meanwhile, graphene decorated by 5d transition metals presents a switchable QAHE, where the out-of-plane/in-plane magnetization can be controlled by an $EEF_\perp$[20]. Somewhat similar control of the topological phase has been predicted for the triphenyl-lead MOF. At the ground state it is characterized by a (antiferromagnetic) topologically trivial phase, and the QAHE takes place mediated by an $EEF_\perp$, which promotes an out-of-plane ferrimagnetic phase[21]. Very recently, Ren *et al.* demonstrated that the in-plane magnetization can induce the QAHE in 2D systems with inversion symmetry, and no (out-of-plane) mirror symmetry[22].
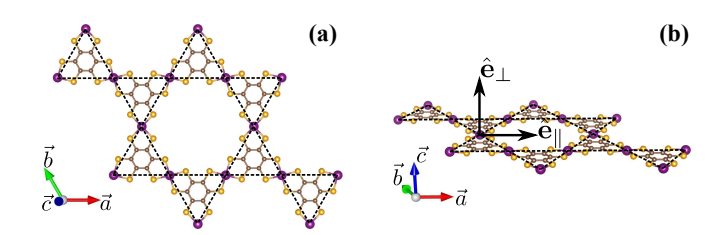

FIG. 1. Atomic structure of the MOF $(MC_4S_4)_3$, top-view (a) and side-view (b), the C atoms are shown in brown, S in yellow and M in purple.

In this work, we use first-principles calculations and tight-binding (TB) models to investigate the electronic and magnetic properties of $(MC_4S_4)_3$ MOFs, with M=Mn, Fe, Co, Ru, and Rh. Fig. 1 shows the structural model of free-standing $(MC_4S_4)_3$. The energetic preference for in-plane versus out-of-plane magnetization was examined through the calculation of the magnetic anisotropy energy (MAE). We found that the out-of-plane magnetization is favored in $(MC_4S_4)_3$ MOFs with M=Mn, Fe, and Ru, giving rise to (intraspin) energy gap induced by the SOC. The QAHE of those MOFs was characterized by the calculation of the Chern number (C), and the formation of topologically protected (metallic) edge states. We show that the Fermi level can be tunned in and out of the non-trivial energy gap with quite feasible electron (n-type) doping. Further MAE calculations, on the electron-doped systems, indicate a strengthening of the out-of-plane magnetization in $(RuC_4S_4)_3$, namely, the MAE increases from 2.0 to 2.8 meV/Ru-atom. Finally, we show that such a n-type doping, and consequently the energy position of the Fermi level, can be controlled on MOF/graphene vdW interfaces through an $EEF_\perp$.

II. METHOD

The calculations were performed based on the DFT approach, as implemented in the VASP code[23]. The exchange correlation term was described using the GGA functional proposed by Perdew, Burke and Ernzerhof (PBE)[24]. The Kohn-Sham orbitals are expanded in a plane wave basis set with an energy cutoff of 400 eV. The 2D Brillouin Zone (BZ) is sampled according to the Monkhorst-Pack method[25], using a gamma-centered 4×4×1 mesh for atomic structure relaxation and 6×6×1 mesh to obtain the self-consistent total charge density. The electron-ion interactions are taken into account using the Projector Augmented Wave (PAW) method[26]. All geometries have been relaxed until atomic forces were lower than 0.025 eV/Å. The metal-organic framework (MOF) monolayer system is simulated considering a vacuum of 16 Å perpendicular to the layers. In order to describe the strong Coulomb interaction between d orbitals of the transition metal, we adopted the GGA+U approach[27]. In the formation of interface with graphene the vdW interaction (vdW-DF2[28]) was considered to correctly describe the system.

III. RESULTS AND DISCUSSIONS

A. Equilibrium geometry and the MAE

The MOF Metal-Bis(dithiolene) has a hexagonal atomic structure with the metal atoms (M) forming a kagome like structure, indicated by the dashed lines in Fig. 1(a). Here, we have considered M = Mn, Fe, Co, Ru

and Rh. The calculated equilibrium lattice constants (a), presented in Table I, matches closely those of the (experimentally synthesized) $(NiC_4S_4)_3$, where $a = 14$–15 Å[8].

In the present $(MC_4S_4)_3$ systems, the QAHE is constrained to an out of plane magnetization of the MOF[22]. The net magnetic moment and its orientation in $(MC_4S_4)_3$ are dictated by the $3d$ and $4d$ orbitals of the transition metals; the preferential magnetic orientation was obtained by computing the magnetic anisotropy energy (E_{MAE}), here defined as $E_{MAE} = E_\perp - E_\parallel$, where $E_\perp$ and $E_\parallel$ are the total energies of the MOFs with the magnetic moment aligned out-of-plane and in-plane, respectively. It is worth noting that the strongly correlated d electrons requires the consideration of the Hubbard correction term. Our results, within the GGA+U approach, of magnetic anisotropy energy (E_{MAE}) and the net magnetic moment (m) as a function of the Hubbard U values, summarized in Table II in Appendix A, reveals that the stabilization of those magnetic properties is achieved for U $\geq$ 3 eV for all studied metals.

The obtained values for the E_{MAE} and m are shown in Table I for U = 3 eV. We find that $(MnC_4S_4)_3$ presents a net magnetic moment of $3.12\,\mu_B$, and easy-axis out-of-plane, $E_{MAE} = 0.62$ meV/Mn-atom, which supports the quantum anomalous phase proposed by Zhao et $al.$[9]. The QAHE has been also predicted in graphene adsorbed by transition metals Fe[29], Co, Rh[18], and Ru[30]. However, in $(CoC_4S_4)_3$ and $(RhC_4S_4)_3$ we found an energetic preference for the in-plane magnetization, $E_{MAE} = -1.84$ meV/Co-atom and -2.06 meV/Rh-atom, thus indicating that the QAH phase is not expected in those MOFs. Meanwhile, $(FeC_4S_4)_3$ and $(RuC_4S_4)_3$ present FM phases with E_{MAE}=0.31 meV/Fe-atom and 2.0 meV/Ru-atom, which points to the emergence of QAH phases in those MOFs.

TABLE I. Lattice parameter a (Å); magnetization m per TM (μ_b/TM); Magnetic Anisotropy Energy $E_{MAE} = (E_\parallel - E_\perp)/N_M$ (Kelvin/TM) positive (negative) are for easy axis perpendicular (parallel) to the layer; work function $\Phi = V_{vac} - E_f$ (eV). All for $U = 3.0$ eV.

MOF	a	m	E_{MAE}	Φ
$(MnC_4S_4)_3$	15.00	3.12	7.2	5.53
$(FeC_4S_4)_3$	14.81	2.15	3.6	5.60
$(CoC_4S_4)_3$	14.67	1.79	-21.4	5.75
$(RuC_4S_4)_3$	15.19	1.86	23.0	5.46
$(RhC_4S_4)_3$	15.07	0.86	-23.9	5.60

B. Qualitative analysis of the magnetic anisotropy

The $(MC_4S_4)_3$ MOFs present a D_{6h} symmetry, giving rise to two sets of doubly degenerated levels at the Γ point, e_{2g} ($d_{x^2-y^2}$ and d_{xy} orbitals), and e_{1g} (d_{xz} and d_{yz} orbitals), and a non-degenerated level a_{1g} (d_{z^2} orbital). The projected density of states (PDOS) of these
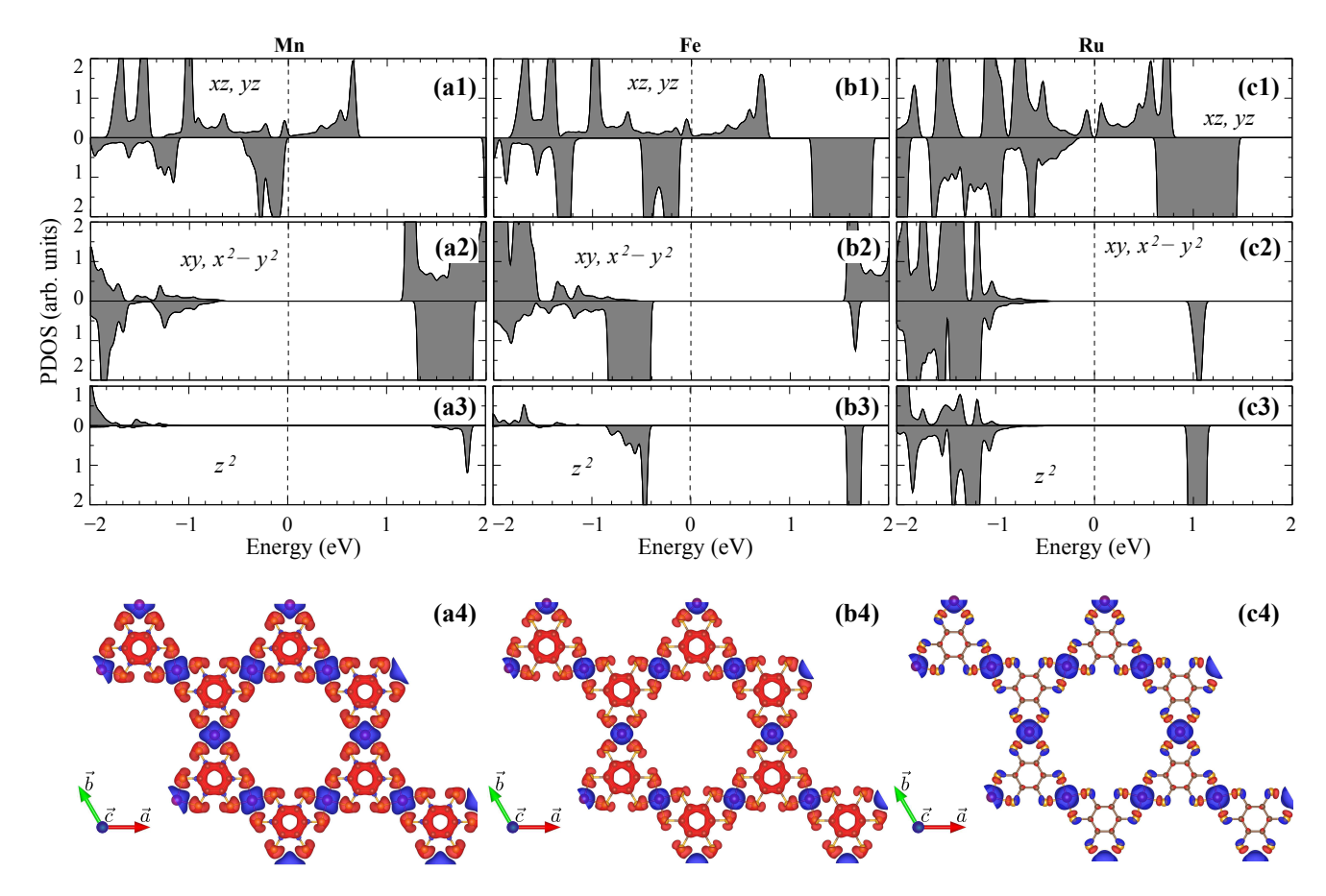
FIG. 2. Spin-polarized projected density of states (PDOS) and the spin-densities of $(MnC_4S_4)_3$ (a1)–(a4), $(FeC_4S_4)_3$ (b1)–(b4), and $(RuC_4S_4)_3$ (c1)–(c4). The spin-density $(\Delta\rho^{\uparrow\downarrow})$ is defined as, $\Delta\rho^{\uparrow\downarrow} = \rho_\uparrow - \rho_\downarrow$, with isosurface of $0.002\,\text{Å}^{-3}$ and blue (red) are regions with net up (down) spin density.

transition metal d orbitals, calculated without SOC, are shown in Fig. 2.

The net magnetization of the MOFs is (i) mostly dictated by the d orbitals of the the transition metals, where about 50% of the magnetic moment comes from the unpaired $d_{xz,yz}$ orbitals, while the out of plane d_{z^2} orbitals contribute with 40% in $(RuC_4S_4)_3$, followed by $(FeC_4S_4)_3$ and $(MnC_4S_4)_3$, 30% and 20%, respectively. As a consequence, (ii) the in plane polarization is larger (lower) in the latter (former) system. Those transition metals are embedded in an organic framework, composed C and S atoms, which present opposite net magnetization ruled by the C-$2p$ and S-$3p$ orbitals; such a (opposite) spin polarization is larger (lower) in $(MnC_4S_4)_3$ $((RuC_4S_4)_3)$. Our spin density results, $\Delta\rho^{\uparrow\downarrow} = \rho_\uparrow - \rho_\downarrow$ [Figs. 2(a4)–(c4)], provide a picture of (i) and (ii) discussed above, and allow us to infer that the FM coupling between the transition metals is given by an indirect exchange process, mediated by the organic host of C and S atoms.

The perturbation approach proposed by Wang *et al.*[31], allow us to use the PDOS above to provide a qualitative analysis of our MAE results[32]. There, the E_{MAE} is approximately defined by the matrix elements of the orbital angular momentum, *i.e.* $\langle u_\sigma | L_z | o_{\sigma'} \rangle$ and $\langle u_\sigma | L_x | o_{\sigma'} \rangle$, where $|o_\sigma\rangle$ and $|u_\sigma\rangle$ refer to the orbital component of the wave-function (e.g. $|\psi\rangle = |u_\sigma\rangle \otimes |\sigma\rangle$) of the occupied ($o$) and empty ($u$) states with a given spin $\sigma = \pm$, calculated without SOC. Namely, the magnetic anisotropy energy can be written as $E_{\text{MAE}} = \Delta E_{\text{d}} + \Delta E_{\text{nd}}$, where the spin diagonal and non-diagonal terms are

$$\Delta E_{\text{d}} = \xi^2 \sum_{\sigma,o,u} \frac{|\langle u_\sigma | L_z | o_\sigma \rangle|^2 - |\langle u_\sigma | L_x | o_\sigma \rangle|^2}{\varepsilon_{u,\sigma} - \varepsilon_{o,\sigma}}, \quad (1)$$

$$\Delta E_{\text{nd}} = \xi^2 \sum_{\sigma,o,u} \frac{|\langle u_\sigma | L_x | o_{\bar{\sigma}} \rangle|^2 - |\langle u_\sigma | L_z | o_{\bar{\sigma}} \rangle|^2}{\varepsilon_{u,\sigma} - \varepsilon_{o,\bar{\sigma}}}, \quad (2)$$

where ξ represents the strength of the SOC. The matrix elements are divided by their (respective) single particle energy difference, indicating that the dominant contributions arise from states near the Fermi level.

For $M = $ Mn, Fe, and Ru, this model tell us that the E_{MAE} is defined by the e_{1g} (d_{xz} and d_{yz} orbitals) orbitals, due to the PDOS peaks near the Fermi level in Figs. 2(a1)–(c1). In these cases, the empty states near the Fermi level are all of the $|u_+\rangle$ type. Moreover, group theory selection rules dictates that L_x matrix operators
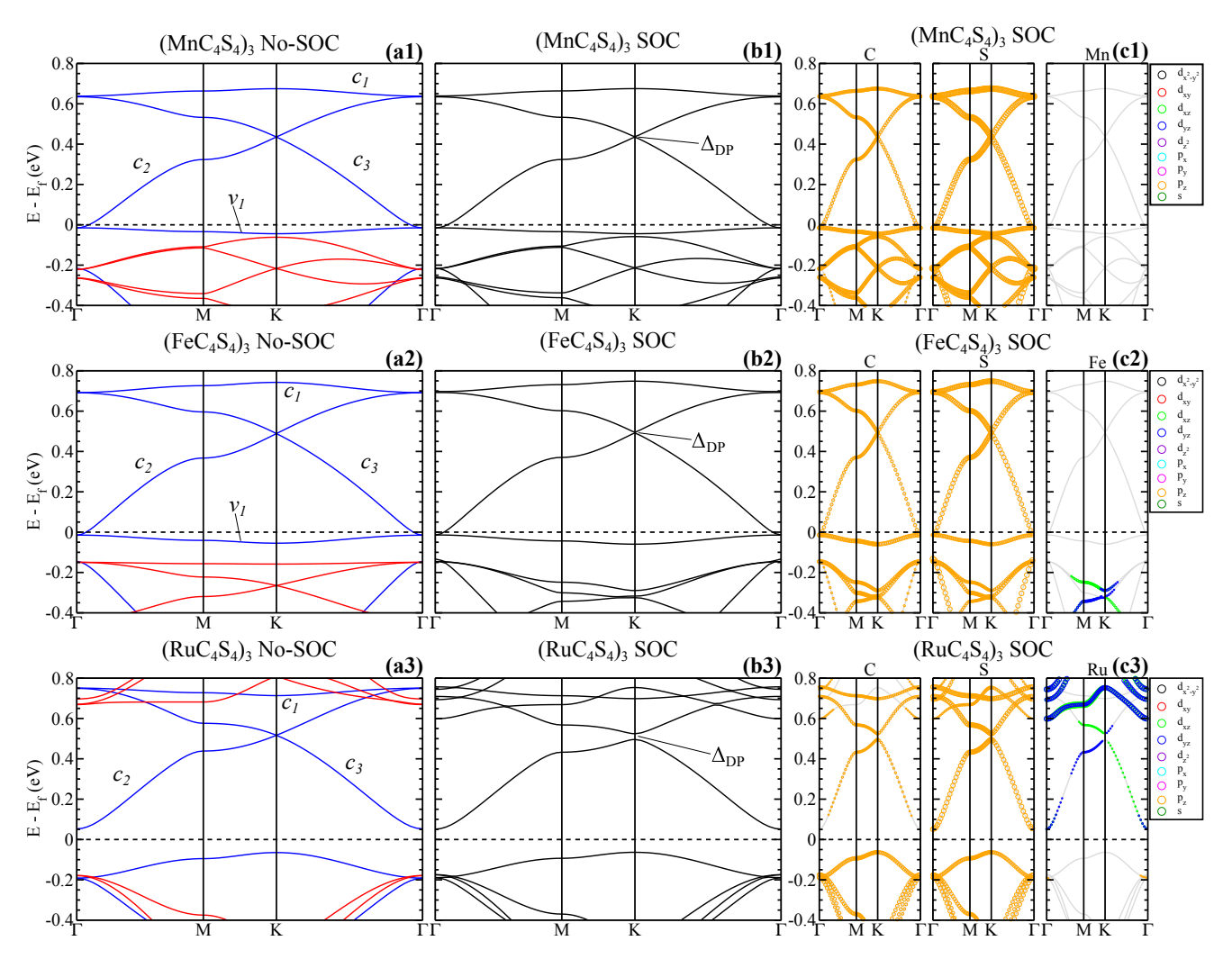
FIG. 3. Electronic band structures of the MOFs, $(MnC_4S_4)_3$, $(FeC_4S_4)_3$, and $(RuC_4S_4)_3$ without SOC (a1)–(a3) where blue (red) are for spin up (down) bands, with SOC (b1)–(b3) and the projected on the atomic orbitals (c1)–(c3).

between e_{1g} states are null. Therefore the dominant contributions are given by the terms $|\langle u_+|L_z|o_+\rangle|^2 - |\langle u_+|L_z|o_-\rangle|^2$ in Eqs. (1)-(2). That is, the sign of E_{MAE} is given by the competition between the positive contribution from the spin-diagonal L_z matrix element, and the negative contribution from the spin-flipped L_z terms. For Ru, Fig. 2(c1), there are no $|o_-\rangle$ contributions near the Fermi level to the PDOS, yielding a large E_{MAE} due to the positive spin-diagonal term. For Fe and Mn, Figs. 2(a1)–(b1), the $|o_-\rangle$ PDOS peaks approach the Fermi level, reducing the E_{MAE}.

C. Kagome bands

The exchange field induced by the transition metals gives rise to (spin-polarized) kagome bands. As shown in Figs. 3(a1)-(c3), those energy bands lie within an energy interval of about $0.8\,eV$ above the Fermi level; characterized by nearly flat bands (c_1 and v_1) degenerated with

Dirac like energy bands, c_2 and c_3. Those energy bands (c_2 and c_3) present linear energy dispersion at the K-point, Dirac point (DP). The electronic band structures of $(MnC_4S_4)_3$ and $(FeC_4S_4)_3$ MOFs reveal a half-metal behavior, characterized by spin-up metallic bands c_2 and c_3 (partially occupied near the Γ-point), and semiconductor spin-down energy bands. Indeed, such a half-metal character in $(MnC_4S_4)_3$ was already reported by Zhao *et al.*[9].

By turning-on the spin-orbit coupling (SOC), we find non-trivial energy gaps of 2 and $3\,meV$ at the Dirac point in $(MnC_4S_4)_3$ and $(FeC_4S_4)_3$, respectively [Δ_{DP} in Figs. 3(b1) and (b2)]. For both systems, the projection on the atomic orbitals [Figs. 3(c1) and (c2)] show that the kagome bands (c_1–c_3 and v_1), are mostly composed by C- and S-p_z orbitals, with no contributions from the Mn and Fe transition metals. In contrast, as shown in Fig. 3(a3), $(RuC_4S_4)_3$ exhibits a semiconducting character for both spin channels. Here the spin-up unoccupied bands form a kagome set of bands (c_1–c_3), with a flat band (c_3) de-
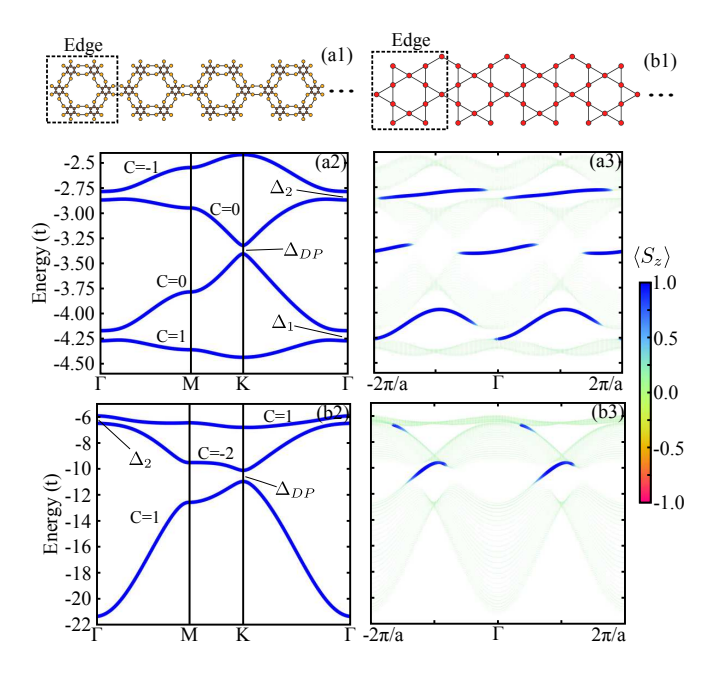
FIG. 4. Lattice structure for the TB model showing the edge geometry for the C-S lattice (a1) and the kagome lattice (b1). 2D bulk band structure for C-S (a2), kagome (b2), and band structure projected edges states for C-S (a3) and kagome (b3). The color bar indicates the spin projection for the bulk and NR band structure.

D.   Quantum Anomalous Hall Effect

In order to provide further support and a more clear physical picture of the QAHE in the MOFs, we calculate the Chern number of $(MC_4S_4)_3$, and examined the formation of topologically protected metallic edge states in $(MC_4S_4)_3$ nanoribbons. The calculations were performed within the TB model by considering one orbital per site. Here, based on the projected energy bands [Fig. 3], we have considered (i) four Hexagonal Multi-Orbital (HMO) bands, composed by the carbon and sulfur (C-S) p_z lattice [Fig. 4(a1)], for the $(MnC_4S_4)_3$ and $(FeC_4S_4)_3$ MOFs; and (ii) Ru kagome lattice model [Fig. 4(b1)] for $(RuC_4S_4)_3$. The TB Hamiltonian can be written as [17,33],

$$H_{TB} = H_0 + H_{SO} + H_M \qquad (3)$$

where H_0 describe the on site energy and nearest and next-nearest neighbor hopping,

$$H_0 = \sum_i \varepsilon_i c_i^\dagger c_i + \sum_{i,j} t_{ij}\, c_i^\dagger c_j, \qquad (4)$$

H_{SO} is the intrinsic spin-orbit coupling of the sites,

$$H_{SO} = i \sum_{i,j} \lambda_{ij}\, c_i^\dagger \boldsymbol{\sigma} \cdot \frac{(\boldsymbol{d}_{kj} \times \boldsymbol{d}_{ik})}{|d_{kj}||d_{ik}|} c_j, \qquad (5)$$

and H_M is a Zeeman exchange field,

$$H_M = b \sum_i c_i^\dagger \sigma_z c_i. \qquad (6)$$

Here $c_i^\dagger = (c_{i\uparrow}^\dagger, c_{i\downarrow}^\dagger)^T$ and $c_i = (c_{i\uparrow}, c_{i\downarrow})^T$, with $c_{i\alpha}^\dagger$ and $c_{i\alpha}$ are the creation and annihilation operators of an electron in the i-th site with spin α; $\boldsymbol{\sigma}$ stands for the Pauli matrices in the spin space. The $\boldsymbol{d}_{ij}$ are the vectors connecting the i-th to the j-th site, ε_i, t_{ij}, λ_{ij} and b controls the on-site, hopping, spin-orbit and Zeeman field strength, respectively. The hopping and spin-orbit terms depend on the distance between the sites, respectively

$$t_{ij} = -Nt \exp\{-\alpha\, d_{ij}\},$$
$$\lambda_{ij} = N\lambda \exp\{-\beta\, d_{ij}\}.$$

We have taken the normalization with respect to the first neighbor distance d_{nn}, $N = \exp(-\alpha d_{nn})$, and $t = 1$; α and β control of the range of the hopping, namely, for larger values $(\gg 1)$ only first neighbor hopping has been considered, while for α, $\beta \ll 1$, further neighbors are taken into account. In Figs. 4(a2)–(b2), we present the the energy bands for the C-S lattice, *i.e.* $(FeC_4S_4)_3$ and $(MnC_4S_4)_3$ [(i)], and the Ru kagome lattice [(ii)], where we find that the main features of the DFT bands have been nicely captured by the current TB approach [34].

Based on the same TB approach, the topological character of the energy gaps was evaluated through the calculation of the Chern number (C). By using the C-S model, as depicted in Fig. 4(a2), we found $C = 1$ for the Fermi level lying in the energy gap Δ_1, keeping the same values for the energy gaps Δ_{DP} and Δ_2. Meanwhile, based on the Ru kagome lattice model, the Chern number is positive $(C = 1)$ at Δ_{DP}, and becomes negative $(C = -1)$ in Δ_2, Fig. 4(b2). It is worth noting that the latter is a local gap at the Γ point, since the energy bands become metallic due to the downward dispersion of the nearly flat kagome band. Since the anomalous Hall conductance is given by $\sigma_{xy} = (e^2/h)C$, it is predicted just one conducting channel per edge for a given energy position of the Fermi level, where opposite edges present conducting channels with opposite carrier velocities $(\nabla\varepsilon(\mathbf{k})/\hbar = \mathbf{v}(\mathbf{k}))$.

Indeed, this is what we found along the edge sites of $(MC_4S_4)_3$ of the NRs. We have considered NR structures with a width of 30 unit cells $(\approx 44, nm)$; and based on the C-S lattice model, in Fig. 4(a3) we present the calculated electronic band structure projected on the edge

generated with two Dirac like bands (c_2, c_3). At $0.52\,eV$ above the Fermi level, the degeneracy of the Dirac point has been removed by the SOC, giving rise to a non-trivial energy gap of $28\,meV$, Δ_{DP} in Fig. 3(b3). Such a larger energy gap, compared with the other MOFs, can be attributed to the hybridization of the Ru-$4d_{xz,yz}$ with the host C- and S-p_z orbitals near the DP of the kagome bands, Fig. 3(c3).

sites of the NR [dashed-square region in the Fig. 4(a1)]. We find only one conducting channel, *i.e.* only one topologically protected edge state associated with each non-trivial energy gap. All of them are characterized by the same direction for the carriers velocities, for instance $\vec{b}$ in Fig. 2, and positive values of $\langle S_z \rangle$. Whereas, the opposite edge of the NR will present carrier velocities in the opposite direction $(-\vec{b})$. Similarly, we find the emergence of topologically protected edge states in $(RuC_4S_4)_3$ NRs described by the Ru kagome lattice model, Fig. 4(b1). As depicted in Fig. 4(b3), those edge states present one single conducting channel with positive values of spin-polarization, and carrier velocities one along the $\vec{b}$ direction, and another one (characterized by a low density of states) with carrier velocities in the opposite direction, $-\vec{b}$. Here, the former is associated with the non-trivial energy gap Δ_{DP} with $C = 1$, while the latter is due to the local non-trivial energy gap Δ_2 with $C = -1$.

E. MOF/G Charge transfer and the control the Fermi level

The manifestation of the QAHE, *i.e.* the appearance of (topologically) protected edge currents, relies on the energy position of the Fermi level with respect to the non-trivial energy gaps. In the present MOFs, as indicated in Fig. 3, we may place the Fermi level in the energy gap Δ_{DP} through electron doping processes. Indeed, this is what we obtained by charging the MOF by about $5 \times 10^{13} e/cm^2$, which is a quite feasible n-type doping. It is worth noting that the net magnetization of the MOFs increases by about the same amount $0.2 \mu_B$, while the MAEs of the charged $(MnC_4S_4)_3$ and $(FeC_4S_4)_3$ MOFs are practically the same when compared with those of the neutral MOFs; whereas in $(RuC_4S_4)_3$, $E_{MAE} = 2.0 \rightarrow 2.8$ meV/Ru-atom. The required doping to achieve the QAH state in the $(RuC_4S_4)_3$ makes the magnetic properties of the system more robust with respect to thermal perturbations. Such a n-type doping can be done through the physisorption of the MOF on metal surfaces with work function smaller compared with that of the MOF; or we may consider an interface engineering based on 2D vdW heterostructures like MOF/graphene.

Graphene is a quite interesting substrate, since it provides both structural stability, and the n-type doping of the MOFs discussed above. The work functions (Φ) of the MOFs (see Table I) are about 1 eV larger compared with the that of graphene. Here we will focus on a particular MOF/graphene interface, $(RuC_4S_4)_3/G$ [35].

First, by considering a set of $(RuC_4S_4)_3/G$ staking geometries, we find that the energetically most stable configuration is characterized by Ru atoms aligned on top of C atoms of the graphene sheet, as seen in Fig. 5(a). The energetic stability of $(RuC_4S_4)_3/G$ was inferred by the calculation of the binding energy $E^b = 8.5$ meV/$Å^2$, which is defined as the total energy difference between the final system $[(RuC_4S_4)_3/G]$ and the sum of the to-
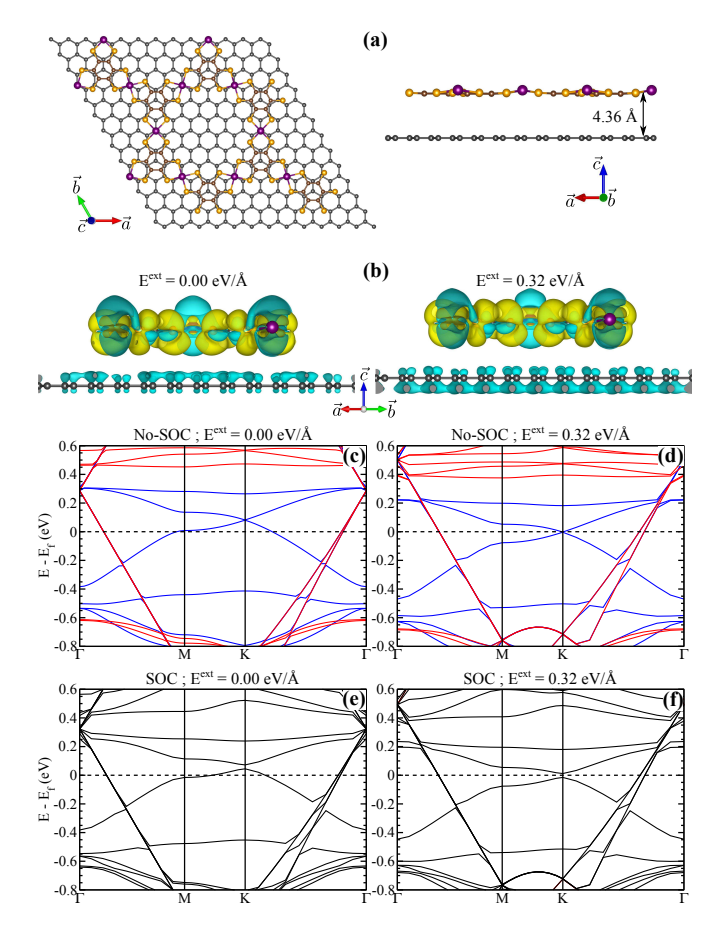

FIG. 5. Atomic structure of $(RuC_4S_4)_3$/Graphene, top-view and side-view (a), and the charge transfer without and with external electric field (b), blue (yellow) indicates regions with loss (gain) of electrons. Electronic band structure without SOC and with external electric field (E^{ext}) of 0.00 (c), 0.32 eV/Å (d) and with SOC and $E^{ext} = 0.00$ (e), $= 0.32$ eV/Å (f).

tal energies of the isolated components, $(RuC_4S_4)_3$ and single layer graphene. It is worth noting that this binding is larger than the one obtained for a graphene bilayer system, 2.2 meV/$Å^2$. At the equilibrium geometry we find an interlayer distance of 4.36 Å, Fig. 5(a), with no chemical bonds at the $(RuC_4S_4)_3/G$ interface.

The larger work function of $(RuC_4S_4)_3$ ($\Phi = 5.46$ eV), compared with the one of graphene, will promote a net charge transfer from graphene to the MOF. In Fig. 5(b) we present a map of such a charge transfer, where the blue (yellow) regions illustrate the loss (gain) of electrons in each layer. Focusing on the electronic properties, based on the first-principles calculations, upon the formation of the $(RuC_4S_4)_3/G$ interface, we find an up-shift of the Fermi level of $(RuC_4S_4)_3$, characterizing the n-type doping of the MOF, whereas the graphene sheet becomes p-type doped, with the Fermi level lying at 0.3 eV below the Dirac point. By turning on the SOC, Fig.5(e), the non-trivial energy gap Δ_{DP} of the MOF is the same compared with the one of isolated system; however, we find

that the Fermi level of the $(RuC_4S_4)_3/G$ system does not lie within Δ_{DP}, and thus, there is no appearance of anomalous Hall current along the edge sites.

In a previous study[17], we verified that the occupation of the kagome bands, as well as the localization of the non-trivial energy gaps in MOF/MOF interfaces, can be controlled by an external electric field. It is worth to pointing out that the energy bands responsible to the QAH phase are completely spin polarized and separated, with the magnetization out of the MOF plane. In such a situation, the Rashba SOC does not affect the gap opened by the intrinsic SOC, thus contrasting with its non-magnetic QSH counterpart[17]. Here, mediated by the MOF↔G charge transfers, the energy bands of the MOF and G system can be tuned by an $EEF_\perp$ (perpendicular to the MOF/G interface). In particular, by increasing the n-type doping of $(RuC_4S_4)_3$ by an $EEF_\perp$ of $0.32\,eV/\text{Å}$, we find the Fermi level lying on the DP of the MOF [Fig. 5(d)]; while the SOC gives rise to Δ_{DP} of $27\,meV$ at the Fermi level, Fig. 5(f), promoting the (topologically) protected edge currents in $(RuC_4S_4)_3/G$, switchable on-and-off through an $EEF_\perp$.

IV. SUMMARY AND CONCLUSION

Based on combined first-principles DFT calculations and the tight-binding models, we have studied the electronic and the topological properties of $(MC_4S_4)_3$ MOFs, with M = Mn, Fe, Co, Ru, and Rh. Our results of magnetic anisotropy energy (MAE) reveal that the $(MC_4S_4)_3$ systems (with M = Mn, Fe and Ru) present the easy axis out-of-plane, while the other metals (Co and Rh) are characterized by an energetic preference for in-plane magnetization. Since both inversion and out-of-plane

mirror reflection symmetries are preserved, the QAH phase is not expected in the latter group[22]. Meanwhile, the QAHE of the former MOF group was verified through the calculation of the (non-zero) Chern number, and the formation of the topologically protected edge states in MOF nanoribbons. Among the currently studied systems, $(RuC_4S_4)_3$ presents the largest energy gap induced by the SOC. Upon n-type doping $(5 \times 10^{13}e/cm^2)$, in order to place the Fermi level in the non-trivial energy gap, we find that the MAE of $(RuC_4S_4)_3$ increases by about 40%, thus improving its magnetic stability with respect to thermal perturbations. Such a tuning of the Fermi level, and the strengthening the out-of-plane magnetization in $(RuC_4S_4)_3$ have been examined by considering the MOF adsorbed on the graphene sheet. The formation of the $(RuC_4S_4)_3/G$ interface is an exothermic process, which may promote the structural stability of the MOF. Further tuning of the Fermi level has been done through an external electric field, $EEF_\perp$, which control the $G \to (RuC_4S_4)_3$ net charge transfer, and the appearance of topologically protected (spin-polarized) edge currents in the MOF. Here, although we have considered a single system, $(RuC_4S_4)_3/G$, we may infer that other MOF/G interfaces can be engineered to exploit/control the QAH properties, like magnetic anisotropy energy and the energy position of the Fermi level.

V. ACKNOWLEDGMENTS

[1] C. L. Kane and E. J. Mele, Phys. Rev. Lett. **95**, 226801 (2005).

[2] Y. Xu, B. Yan, H.-J. Zhang, J. Wang, G. Xu, P. Tang, W. Duan, and S.-C. Zhang, Phys. Rev. Lett. **111**, 136804 (2013).

[3] N. D. Drummond, V. Zólyomi, and V. I. Fal'ko, Phys. Rev. B **85**, 075423 (2012).

[4] J. E. Padilha, R. B. Pontes, T. M. Schmidt, R. H. Miwa, and A. Fazzio, Scientific Reports **6**, 26123 (2016).

[5] X. Qian, J. Liu, L. Fu, and J. Li, Science **346**, 1344 (2014).

[6] Z. F. Wang, Z. Liu, and F. Liu, Phys. Rev. Lett. **110**, 196801 (2013).

[7] Z. F. Wang, N. Su, and F. Liu, Nano Letters **13**, 2842 (2013), pMID: 23678979.

[8] T. Kambe, R. Sakamoto, K. Hoshiko, K. Takada, M. Miyachi, J.-H. Ryu, S. Sasaki, J. Kim, K. Nakazato, M. Takata, and H. Nishihara, Journal of the American Chemical Society **135**, 2462 (2013).

[9] M. Zhao, A. Wang, and X. Zhang, Nanoscale **5**, 10404 (2013).

[10] A. Wang, X. Zhang, Y. Feng, and M. Zhao, The Journal of Physical Chemistry Letters **8**, 3770 (2017), pMID: 28762733.

[11] H. Maeda, R. Sakamoto, and H. Nishihara, Langmuir **32**, 2527 (2016), pMID: 26915925.

[12] H. Alves, D. Simão, I. Cordeiro Santos, V. Gama, R. Teives Henriques, H. Novais, and M. Almeida, European Journal of Inorganic Chemistry **2004**, 1318 (2004).

[13] J. W. Colson and W. R. Dichtel, Nature Chemistry **5**, 453 (2013), review Article.

[14] D. Sheberla, L. Sun, M. A. Blood-Forsythe, S. Er, C. R. Wade, C. K. Brozek, A. Aspuru-Guzik, and M. Dincă, Journal of the American Chemical Society **136**, 8859 (2014), pMID: 24750124.

[15] D. Rodriguez-San-Miguel, P. Amo-Ochoa, and F. Zamora, Chem. Commun. **52**, 4113 (2016).

[16] R. Sakamoto, K. Takada, X. Sun, T. Pal, T. Tsukamoto, E. J. H. Phua, A. Rapakousiou, K. Hoshiko, and H. Nishihara, Coordination Chemistry Reviews **320-321**, 118 (2016), sI: Functional Nanomaterials 2016.

[17] F. C. de Lima, G. J. Ferreira, and R. H. Miwa, Phys. Rev. B **96**, 115426 (2017).

[18] J. Hu, Z. Zhu, and R. Wu, Nano Letters **15**, 2074 (2015), pMID: 25689149.

[19] L. Dong, Y. Kim, D. Er, A. M. Rappe, and V. B. Shenoy, Phys. Rev. Lett. **116**, 096601 (2016).

[20] H. Zhang, C. Lazo, S. Blügel, S. Heinze, and Y. Mokrousov, Phys. Rev. Lett. **108**, 056802 (2012).

[21] H.-J. Kim, C. Li, J. Feng, J.-H. Cho, and Z. Zhang, Phys. Rev. B **93**, 041404 (2016).

[22] Y. Ren, J. Zeng, X. Deng, F. Yang, H. Pan, and Z. Qiao, Phys. Rev. B **94**, 085411 (2016).

[23] G. Kresse and J. Furthmüller, Computational Materials Science **6**, 15 (1996).

[24] J. P. Perdew, K. Burke, and M. Ernzerhof, Phys. Rev. Lett. **77**, 3865 (1996).

[25] H. J. Monkhorst and J. D. Pack, Phys. Rev. B **13**, 5188 (1976).

[26] P. E. Blöchl, Phys. Rev. B **50**, 17953 (1994).

[27] S. L. Dudarev, G. A. Botton, S. Y. Savrasov, C. J. Humphreys, and A. P. Sutton, Phys. Rev. B **57**, 1505 (1998).

[28] K. Lee, E. D. Murray, L. Kong, B. I. Lundqvist, and D. C. Langreth, Phys. Rev. B **82**, 081101 (2010).

[29] Z. Qiao, S. A. Yang, W. Feng, W.-K. Tse, J. Ding, Y. Yao, J. Wang, and Q. Niu, Phys. Rev. B **82**, 161414 (2010).

[30] C. M. Acosta, M. P. Lima, R. H. Miwa, A. J. R. da Silva, and A. Fazzio, Phys. Rev. B **89**, 155438 (2014).

[31] D.-s. Wang, R. Wu, and A. J. Freeman, Phys. Rev. B **47**, 14932 (1993).

[32] Y. Song, X. Wang, and W. Mi, Phys. Rev. Materials **1**, 074408 (2017).

[33] E. Tang, J.-W. Mei, and X.-G. Wen, Phys. Rev. Lett. **106**, 236802 (2011).

[34] For the (C–S) hexagonal multi-orbital [(i)] we have considered the following parameterization, $a = 14.8$ Å, $\varepsilon_C = 0\,t$, $\varepsilon_S = 0.5\,t$, $\lambda = 0.1\,t$, $b = -1.5\,t$ and $\alpha = \beta = 0.6$ Å^{-1}; and for the Ru kagome lattice [(ii)] we have used, $\varepsilon = 0\,t$, $\lambda = 0.4\,t$, $b = -5.0\,t$ and $\alpha = \beta = 0.3$ Å^{-1}.

[35] In order to satisfy the periodic boundary conditions, within our supecell approach, the graphene sheet was described by using a supercell with periodicity of (6×6), giving rise to lattice mismatch of 2.9%.

Appendix A: GGA+U

In Table II we summarize our results of magnetic anisotropy energy ($E_{\mathrm{MAE}} = (E_{\parallel}-E_{\perp})/N_{\mathrm{M}}$) of $(MC_4S_4)_3$ for M=Mn, Fe, Co, Ru, and Rh. Qualitatively, our results do not depend on the value of U, which is only required for the quantitative description of the metal d orbitals.

TABLE II. Magnetic Anisotropy Energy E_{MAE} (in meV/M-atom) and the magnetization (m) of the unity cell per transition metal (M), for $(MC_4S_4)_3$ (M= Mn, Fe, Co, Tc, Ru, Rh), as a function of U ($U = 2-4$), positive (negative) are for easy axis $\hat{\mathbf{e}}_{\perp}$, perpendicular ($\hat{\mathbf{e}}_{\parallel}$, parallel) to the layer.

U	2 eV		3 eV		4 eV	
MOF	MAE	m	MAE	m	MAE	m
$(MnC_4S_4)_3$	0.63	3.06	0.62	3.12	0.61	3.18
$(FeC_4S_4)_3$	0.28	2.90	0.31	2.15	0.39	2.22
$(CoC_4S_4)_3$	-1.61	1.11	-1.84	1.17	-2.08	1.23
$(RuC_4S_4)_3$	2.14	1.78	1.98	1.86	1.84	1.92
$(RhC_4S_4)_3$	-1.29	0.79	-2.07	0.86	-3.00	0.90